

Transfer Efficiency for an Oil Spray Application

W. Kalata^{*}, K. Brown, S. O'Donnell and R. J. Schick
Spray Analysis and Research Services
Spraying Systems Co.
Wheaton, IL 60187-7901 USA

Abstract

Many food products utilize spray coatings to boost the value of the product by making production more efficient or improving; flavor, appearance, shelf life, and many others attributes. This work focuses on the application of thin coatings of vegetable oils as an ingredient or as a release agent for food grade molds. Maximizing transfer efficiency is a key focus in oil spray applications in order to reduce costs, material waste, and adverse health hazards of overspray.

This study is focused on the development of a robust method of accurately simulating the application of vegetable oils. An experimental design approach was employed to measure and validate critical parameters of the peanut oil spray system. A combination of Particle Image Velocimetry (PIV), Laser Induced Florescence (LIF), and Phase Doppler Interferometry (PDI) was performed under controlled laboratory conditions. Testing was carried out with various hydraulic nozzles and operating conditions. In some instances, a custom conveyance system was used to move the substrate below the nozzle header at low speeds. Experimental results show that heated oil had better transfer quality. In terms of transfer efficiency preliminary observations show that increases in pressure and temperature decrease the transfer efficiency due to an increase in material loss to free roaming small droplets.

The computational fluid dynamics (CFD) simulations were conducted using the ANSYS Fluent package in conjunction with methods developed at Spraying Systems Co. The computational model's agreement, and disagreement, with the experimentally acquired results provides insight for the appropriate considerations when constructing simulations to evaluate coverage and transfer efficiency.

* Corresponding author: Wojciech.Kalata@spray.com

Introduction

In many food processing applications vegetable oils are applied with the use of hydraulically atomized spray nozzles to food products as an ingredient or to pans as a release agent. Most commonly, the application is done on a conveyance system requiring repeatable output. Optimal coating is uniform across the spray pattern and must react to product size/shape, conveyor speed, temperature, humidity and multiple chemistries. A uniform coating and repeatable output is imperative to producing high quality products.

In order to improve profitability, the cost per unit must be reduced while maintaining or improving product quality. During the atomization process, droplets are formed that can drift into surrounding areas rather than transferring to the intended target. This is known as overspray, which contributes to waste and can potentially be an environmental hazard. Drops smaller than ten microns can be inhaled and create an inhalation risk to operators. Hence, there are substantial economic and environmental reasons to increase the transfer efficiency of oil from the nozzle to the product.

Transfer efficiency is defined as the ratio of the weight of coatings material deposited on a substrate to the total weight of coatings solids used in a coating application step, expressed as a percentage [1]. The atomization process is the primary source of material loss in this type of application, which requires careful attention and quantification of over-spray.

The atomization process in hydraulic nozzles is significantly affected by the viscosity of the fluid [2]. These effects are of particular concern in coating applications, as the viscosity effects can result in non-uniform distribution of the spray pattern. This translates directly to poor product quality.

Various testing techniques in conjunction with computational fluid dynamics (CFD) allowed for a rigorous engineering assessment and design of optimized spray based systems. The focus of the present study was to analyze the common effects of heavy edging and misting for hydraulic flat sprays which reflect on the liquid transfer efficiency. This study experimentally investigated drop size, droplet velocities, and spray pattern concentration under varying conditions of spray angle, nozzle capacity, pressures, and temperatures. Additionally, CFD was performed on the flat fan spray nozzles and spray environment to analyze liquid velocity and concentration.

Methods

Process Conditions

The experimental setup focused on a Spraying Systems Co. UniJet[®] body with four different hydraulic flat-fan type spray tips: TPU-80-0050, TPU-80-01, TPU-110-0050 and TPU-110-01 (shown in Figure 1). These four tips are rated at two different fan angles (80 and 110 degrees at 40 psi), and two different flow capacities (0.05 and 0.1 gpm at 40

psi for water). Hence the case naming convention correlates to the rating of the spray tips.

The liquid investigated in this work was peanut oil. Among various vegetable oils, this oil is one of the most common oils sprayed in the conveyed coverage type applications. The scope of this study included data collections at two oil temperatures and two spray differential pressures, resulting in four conditions in total. The oil was sprayed at both the ambient laboratory temperature of 21.1°C (70°F) and at a heated temperature of 43.3°C (110°F). The temperature measurements were made by probing the peanut oil of the liquid feed line immediately before exiting the nozzle. Two spray differential pressure conditions were at 3.8 bar (55 psi) and 4.8 bar (70 psi). Since temperature was one of the variables in this study, the density and viscosity of peanut oil changed, hence, oil flow rate changed as well. The operating parameters and peanut oil material properties for all tests are noted in Table 1. In all tests, the oil was sprayed vertically down.

Standard and High Speed Video

Standard video was taken of the spray at all testing conditions spraying on both stagnant and conveyed surfaces. The surface being sprayed on was positioned perpendicular to the downward direction of the nozzle, located 15.24 cm (6 in) directly beneath the nozzle tip. The conveyor surface travelled at 0.305 m/s (1 ft/s).

The Olympus i-SPEED TR high speed video camera was used for capturing High Speed Video (HSV) during stagnant surface tests of TPU-110-01 nozzle. The oil temperature was at 21.1°C and 43.3°C, and the pressure set at 4.8 bar. Videos were taken at 1500 fps at resolution of 1280x1024. Two sets of videos were taken. The first set focused on half of the spray fan. The second set focused on the distinctive heavy spray edge impacting the surface and splashing.

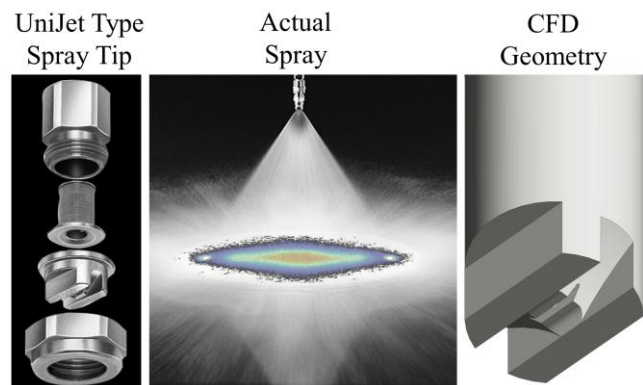


Figure 1. Spiral type spray nozzle (actual nozzle – left and middle, CFD geometry – right).

Phase Doppler Particle Analyzer

A two-dimensional TSI Phase Doppler Particle Analyzer (PDPA) system was used for this study to acquire drop size and velocity measurements across half of the flat fan spray,

Conditions	Units	TPU 80-0050	TPU 80-01	TPU 110-0050	TPU 110-01
T = 21.1°C, P = 3.8 bar					
Mass Flow Rate	g/s	3.33	6.89	3.15	6.94
Density	kg/m ³			912.4	
Dynamic Viscosity	cP			72.0	
Surface Tension	N/m			0.0326	
T = 21.1°C, P = 4.8 bar					
Mass Flow Rate	g/s	3.81	7.85	3.76	7.67
Density	kg/m ³			912.4	
Dynamic Viscosity	cP			72.0	
Surface Tension	N/m			0.0326	
T = 43.3°C, P = 3.8 bar					
Mass Flow Rate	g/s	3.53	7.08	3.45	6.97
Density	kg/m ³			897.6	
Dynamic Viscosity	cP			31.6	
Surface Tension	N/m			0.0305	
T = 43.3°C, P = 4.8 bar					
Mass Flow Rate	g/s	4.03	8.07	3.94	7.93
Density	kg/m ³			867.6	
Dynamic Viscosity	cP			31.6	
Surface Tension	N/m			0.0305	

Table 1. Peanut oil conditions for various pressures, temperatures and nozzle configurations.

measured from the nozzle center to the edge of the spray (Figure 2). The PDPA system provides a single point-measurement; therefore, data was collected at multiple points across each spray fan. The data was then post-processed into volume flux averaged values.

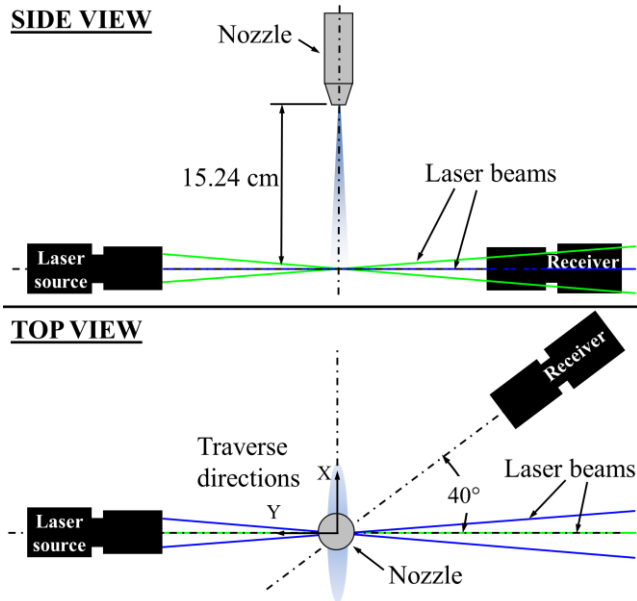


Figure 2. Setup for the PDPA measurements.

A 300 mWatt Argon-Ion laser provided the light source. The laser provides approximately 50 – 60 mW of power per beam. The laser light transmitter and receiver were mounted on a rail assembly with rotary plates along with the light receiver oriented in a 40° forward scatter collection position. The laser was operated at an adequate power setting to overcome error due to interfering spray density effects.

For these particular tests, a transmitting lens with a 500 mm focal length and a receiving lens with a 1000 mm focal length were selected for optimum drop size resolution. This resulted in an optimized size range of approximately 2 μm – 930 μm droplets. This optical setup ensured capturing the full range of droplet sizes while maintaining adequate measurement resolution. The designated range used during the trial was determined by a preliminary test in which the Volume Median Diameter (VMD or $D_{V0.5}$) and the overall droplet distribution were examined. This verified that the lens selection was adequate to capture the entire range of droplet size produced by the nozzles. For each test point a maximum of 10,000 samples were acquired. For further explanation of drop size terminology refer to Lefebvre [3].

The drop size and velocity measurements were performed 15.24 cm (6 in) from the tip of the nozzle, as shown in Figure 2. The intersection point of the x and y axes was directly underneath the center of the nozzle. With an assumption of symmetry, the drop size measurements were taken from the center of the nozzle to the edge of the spray fan. Since it was difficult to get consistent data at the heavy edges of the spray, the drop size measurements excluded the heavy edged region of the spray plume. Only the vertical velocity (V_z) component was measured. A calculation was performed based on the position away from nozzle both in x and z directions to find $|V|$ from the V_z measurement.

Laser Sheet Imaging

The Laser Sheet Imaging (LSI) system used in this study included a Solo PIV Nd:YAG dual laser, high-speed LaVision Imager Intense camera, and Davis 8.0 image acquisition and processing software by LaVision. The LSI system utilized a laser sheet, with a Gaussian intensity profile, which illuminated the spray in a single downstream horizontal plane. The laser sheet was approximately 5 mm thick which was sufficiently thin to represent a two

dimensional sheet in the spray. Images were acquired in the x-y plane. The camera was located at an off-axis angle as shown in Figure 3. The image calibration was conducted by capturing an image of a calibration-sheet with markings of known size and spacing to characterize and correct the skewed camera images to the actual planar spray cross-section and to assign real world dimensions to captured image.

Mie scattering LSI can accurately map spray concentration across a two-dimensional spray pattern under specific spray conditions including: single fluid sprays, uniform drop size, and low density sprays. In Mie scattering the intensity of light emitted from illuminated droplets is directly proportional to the surface area of the droplet. If uniform drop size can be assumed, light intensity can be directly related to liquid volume concentration.

The relatively high viscosity of peanut oil creates a large range of drop sizes when sprayed hydraulically through a fan-type spray tip, thus rendering Mie scattering insufficient for characterizing volumetric distribution. To overcome this problem Laser Induced Fluorescence (LIF) was implemented. In LIF the test fluid is doped with a fluorophore. In this case Rhodamine WT, a fluorescent dye that has a peak absorption of 530 nm and a peak emittance of 555 nm, was ideal for the 532 nm (green) laser that was used in this experiment. When laser light hits Rhodamine WT molecules the dye is excited and emits light at a longer wave length than the supplied laser light. A filter was placed on the camera to suppress wave lengths shorter than 540 nm. This ensured that only the light emitted from the Rhodamine WT reached the camera. Implementing this technique eliminated drop size from influencing the emitted light intensity and instead the light intensity was directly proportional to the number of phosphorous molecules. Once the dye was evenly dispersed in the peanut oil, LIF was a true measurement of liquid concentration across the two-dimensional spray pattern cross-section.

A minimum of 200 instantaneous (very short exposure time) images were acquired for each test condition, subsequent processing to suppress background noise and time-averaging was performed. A time averaged image of the spray pattern allows for a well-defined concentration map of the spray pattern. The laser sheet was located 15.24cm from the tip of the nozzle as shown in Figure 3. An intersection point of x and y-axes was directly underneath the center of the nozzle. This time the coordinate system indicating positive x-y positioning was rotated 180 degrees.

For many vegetable oil spray applications, the substrate being sprayed is on a conveyer moving along the y axis. For conveyer based systems it becomes useful to convert the volumetric distribution to a 1-D coverage profile in the x-direction. This was calculated by summing the pixel-intensities in the y-direction, as seen in Figure 10.

Particle Image Velocimetry

Particle Image Velocimetry (PIV) was used to create a velocity vector map of a two dimensional cross section of the spray plume as shown in Figure 4. Measurements were

taken with the same equipment as previously described for the LSI. The laser sheet was positioned to intersect the center of the spray plume in the y-direction with the center of the height of the laser positioned for minimum laser attenuation at 15.24 cm spray height. The atomized droplets of the spray plume were used as tracer elements for the PIV measurement.

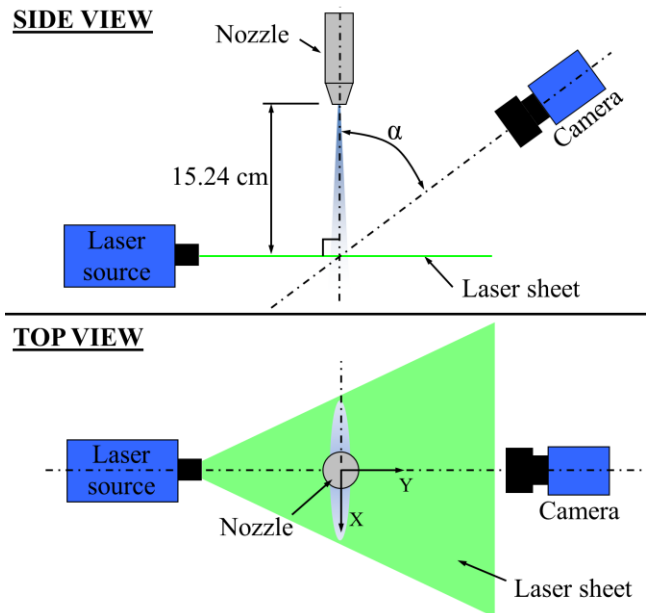


Figure 3. Setup for the LSI measurements.

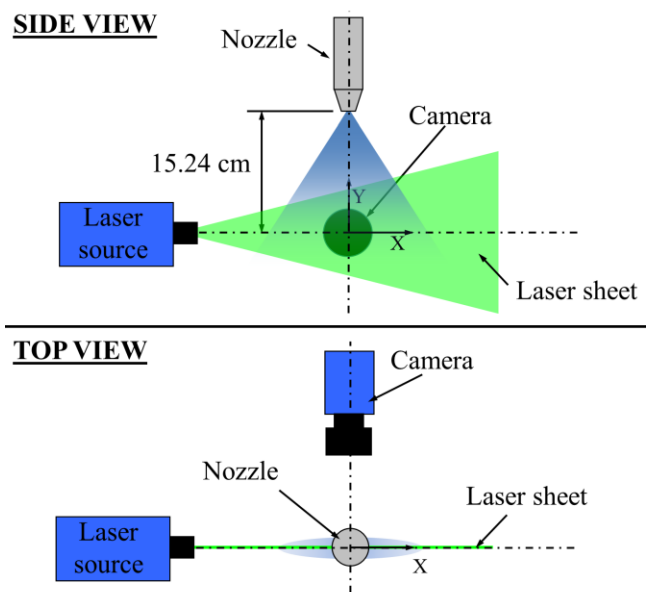


Figure 4. Setup for the PIV measurements.

Two laser shots and simultaneous image acquisition were recorded between 100 μ s and 200 μ s apart, depending on the test conditions, to achieve an average of a 5-10 pixel shift in the droplets in the target region of 15.24 cm from the spray tip. A minimum of 200 PIV image pairs were taken at each test condition. Each pair of images were

processed to create a velocity vector map of the two dimensional cross-section. The velocity vector maps were then averaged. Only velocities inside the range averaged ± 1 RMS were included in the averaging calculation. A one dimensional velocity profile, for both V_z and $|V|$, was extracted from the averaged image at the desired 15.24 cm spray height.

Computational Setup – Initial Considerations

All CFD simulations were performed with ANSYS Fluent version 15. The CFD model was reproduced according to the testing conditions where the nozzle orientation was aligned with experimental conditions. The TPU-110-01 nozzle geometry, which features characteristic v-cut at the tip of the nozzle, was created using 3-D modeler (Autodesk Inventor 2013). This geometry is shown on the right side of Figure 1.

Meshing was performed within ANSYS Workbench 15 using the automated meshing tools. Once unstructured and mixed cells mesh was created, it was transformed into the polyhedral mesh. The polyhedral meshes allow for easier and faster convergence of the solution [4].

In order to further reduce computational load, the 3-D nozzle geometry was split into two domains. The first domain was created to simulate oil flow internally and in the external region in close vicinity of the nozzle. A second domain was created from the Inlet BC profile location down to 15.24 cm away from the nozzle.

Computational Setup – Inlet BC Profile

Initially, an unstructured grid was composed of 3.711 million mixed cells which employed boundary layer type inflation at all walls and utilized a sizing function at the v-cut of the nozzle. Inside FLUENT the unstructured mesh was converted into polyhedral grid while the boundary layer mesh remained. The grid was reduced to 1.087 million polyhedral cells.

This case was set up with liquid mass flow ($7.925e-3$ kg/s) at the inlet boundary condition (BC). This condition corresponded to $T_{oil}=43.3^\circ\text{C}$ and $P_{oil}=4.8$ bar (see Table 1). The outlet BC was set at a Constant Pressure of 0 bar (1.01 bar absolute or reference pressure). Walls were treated with non-slip BC.

Along with the Volume of Fluid (VOF) model, the Transition SST Turbulence model was used. The simulations were performed in steady state mode, which lead to an implicit scheme for the VOF model [4]. The simulation rendered an Inlet BC (see Figure 5) for external flow simulation and confirmed oil pressure differential (4.69 bar – 68.1 psi). At the profile location velocity averaged at 13.2 m/s. The maximum velocity reached 15.7 m/s. This resulted with a Reynolds Number (Re) of 380, hence flow regime at the profile was considered laminar.

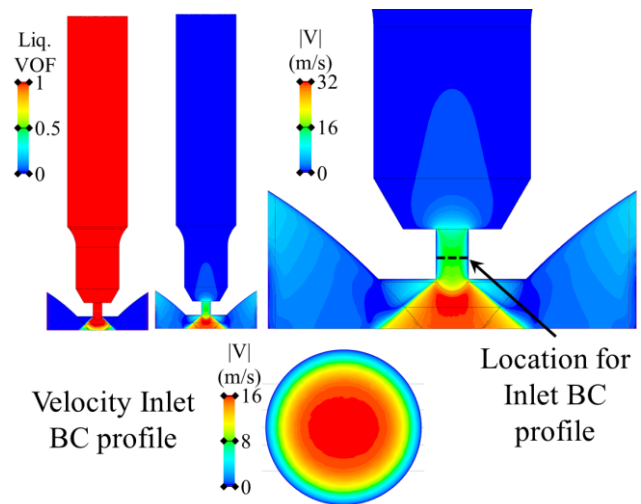


Figure 5. Initial simulation for inlet BC profile.

Computational Setup – External Flow

Similarly to the previous simulation, an unstructured grid was composed of 7.680 million mixed cells which employed boundary layer type inflation at all walls and utilized sizing function at the v-cut the nozzle. Inside FLUENT, the unstructured mesh was converted into polyhedral grid while the boundary layer mesh remained. The grid was reduced to 1.614 million polyhedral cells.

The velocity inlet BC was based on the velocity profile from Figure 5. Each velocity component was loaded separately to ensure that secondary flow effects were included. The outlet pressure BC was setup as constant zero pressure with standard 1.01 bar operating pressure and properly setup gravity term. Nozzle walls were set as rigid, with no-slip conditions. The oil fluid properties were kept the same as in the previous simulation.

Unlike the previous simulation, transient formulation was employed. Again implicit formulation of the VOF model was used. For turbulence modelling a Large Eddy Simulation (LES) Model with WALE Subgrid Scale was used. The transient scheme used iterative Bounded Second Order Implicit formulation. The time step was set to $2.5e-5$ s. 20 iterations per time step were used. Every fourth time step ($\Delta t = 0.0001$ s), series of grayscale images were exported for further image analysis and animation. Data was stored every 0.01 s. The simulation was run for a total of 0.1 seconds.

Experimental Results and Discussion

Imaging with Standard and HSV

Standard videos did not show noticeable differences between a static surface and the conveyed surface. This can be explained due to the fact that velocity of droplets (as shown later) impacting surface are one order of magnitude higher than conveyed surface (0.305 m/s). All videos clearly demonstrated misting and different spray angle corresponding to each nozzle at different conditions (See Figure 6). Also all videos showed heavy edges on the sides of the spray fan. These heavy edges are undesirable effects in this family of nozzles that become more pronounced with increasing viscosity.

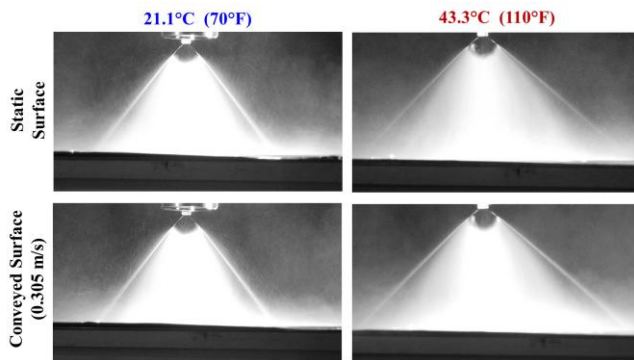


Figure 6. Single frames from standard videos of TPU-110-01 at 4.8 bar with two different temperatures and while spraying onto static and conveyed surfaces.

HSV was useful to observe in detail how spray formed initially, what happened to the droplets during the in-flight stage, and lastly how they impacted the surface. Temperature effects were clearly visible in spray fan angle, where warmer oil spray had larger spray angle as shown in Figure 7. Heavy edges of the spray were observed as well. The HSV was very useful in comparing and validation of transient CFD simulation of the spray.

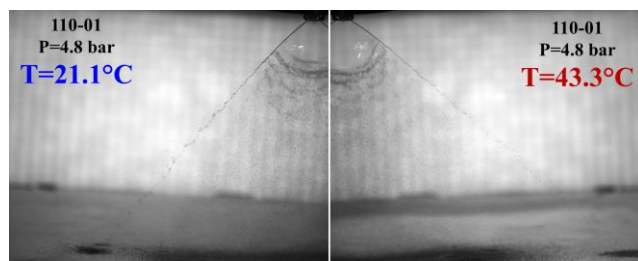


Figure 7. High speed imaging snapshots of TPU-110-01 spray at two different temperatures both at 4.8 bar.

Drop Size and Velocity from PDPA

Table 2 summarizes the PDPA results. For warmer oil temperatures, for every nozzle, there was a consistent reduction in drop sizes when looking at SMD and VMD. Yet the difference was mainly on order of less than 10 microns for VMD, and similarly for SMD. On the other hand, the droplet velocities consistently decreased as the

temperature of oil was increased. This made sense since smaller particles decelerated more rapidly. The Weber number (We) seen in Table 1 was calculated based of Equation 1.

$$We = \frac{\rho |V|^2 D_{V0.50}}{\sigma} \quad (1)$$

To reiterate, drop size and velocity data excluded the heavy edged region. Generally within the region without edges, the drop size profiles were relatively flat therefore volume flux weighing did not affect arithmetic average significantly. The droplet velocity had some variance in profile; hence volume-flux weighting was needed.

LSI

The 2-D spray distribution profiles obtained via LSI-LIF provided many insights into the dynamic environment changes due to oil temperature, pressure, and spray fan angle. All 16 cases of spray distribution are presented in Figures 8 and 9. Figure 8 shows 80° spray angle rated nozzles and Figure 9 shows 110° spray angle rated nozzles. The spray distribution profiles did not fit onto the laser sheet for three of the conditions; therefore half of profiles at a time were obtained and were joined together accordingly in post-processing. This stitching can be noticed in Figure 9 for 110-01 tips at 43.3°. For 110-0050 tip at 4.8 bar and 43.3°C, there was only one side of profile obtained. For esthetic plotting reasons, the second half was mirrored from the first half, due to the symmetry assumption.

The high intensity dots on of the outer most regions of each 2-D pattern in Figures 8 and 9, are the result of heavy edges. As noted earlier these edging features may not be desirable when considering precision spraying where spray distribution play an important role in conveyed coverage. Further difficulty arises when spray overlapping is considered for applications with multiple nozzle manifolds.

Figures 8 and 9 clearly show that increasing temperature results in increasing spray width and capacity, as the intensity of counts directly correlates to the oil flow rate. To quantify the spray width and to characterize conveyer applications, the summed 1-D profiles were obtained as shown in Figure 10. Each profile consisted of heavy edge peaks (marked with red dotted lines as seen on Figure 10) and main profile distribution (between the green dotted lines marked on Figure 10). The spray width of each condition is shown in the bar plot of Figure 11. As seen in Figure 11, the spray width increase has stronger dependence on oil temperature than on oil pressure.

In some instances, transfer efficiency can be related to the heavy edging. The transfer efficiency edging factor (EF%) can be calculated using Equation (2), defined as the percentage ratio of desired summed counts (profile between green dotted lines shown in Figure 10) and total summed counts.

Nozzle	P (bar)	T (°C)	D ₃₂ (µm)	D _{V0.01} (µm)	D _{V0.50} (µm)	D _{V0.99} (µm)	V (m/s)	We
TPU-80-0050	3.8	21.1	92	26	107	330	5.78	100
	4.8		83	23	96	363	7.18	138
	3.8	43.3	81	25	87	352	5.63	82
	4.8		72	24	77	337	5.91	79
TPU-80-01	3.8	21.1	105	28	129	365	7.01	178
	4.8		88	25	100	347	8.12	185
	3.8	43.3	84	25	94	337	6.96	135
	4.8		79	24	86	373	7.99	162
TPU-110-0050	3.8	21.1	86	27	93	338	3.40	30
	4.8		78	25	83	347	3.77	33
	3.8	43.3	79	26	85	327	3.63	33
	4.8		71	23	77	313	4.37	43
TPU-110-01	3.8	21.1	91	28	101	336	5.22	77
	4.8		83	26	91	353	6.32	102
	3.8	43.3	84	27	90	338	5.17	71
	4.8		75	24	81	283	5.92	84

Table 2. Volume flux weighted drop size and velocity results obtained via PDPA.

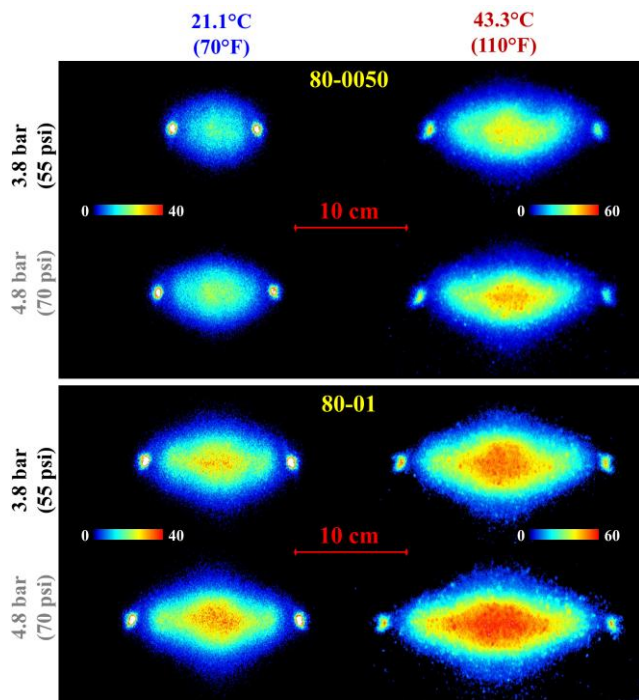


Figure 8. Planar spray distributions from LSI measurements for 80 degree fan angle nozzles.

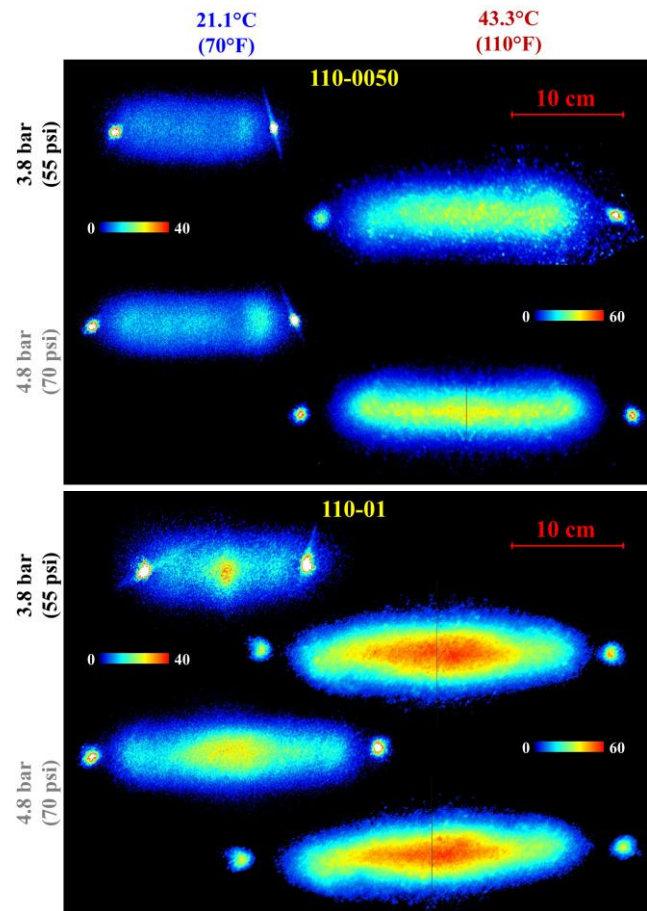


Figure 9. Planar spray distributions from LSI measurements for 110 degree fan angle nozzles.

$$EF\% = 100 \cdot \frac{\sum C_{Desired}}{\sum C_{Full}} \quad (2)$$

This correlated to the percentage of oil volume that is sprayed in a controlled manner, i.e. without oil that goes into heavy edging. Figure 12 shows EF% for all cases. Again, it shows clear benefits of spraying heated peanut oil. All cases with T_{oil} at 43.3°C, had edging factor of 94% or higher. Conversely, the worst case for unheated oil, the 110-01 at 3.8 bar and 21.1°C, resulted in an edging factor of 72%. Further examination of LIF data could lead to quantification of transfer losses due to misting. Increases in temperature and pressures both result in higher levels of misting which could result in lower transfer efficiency.

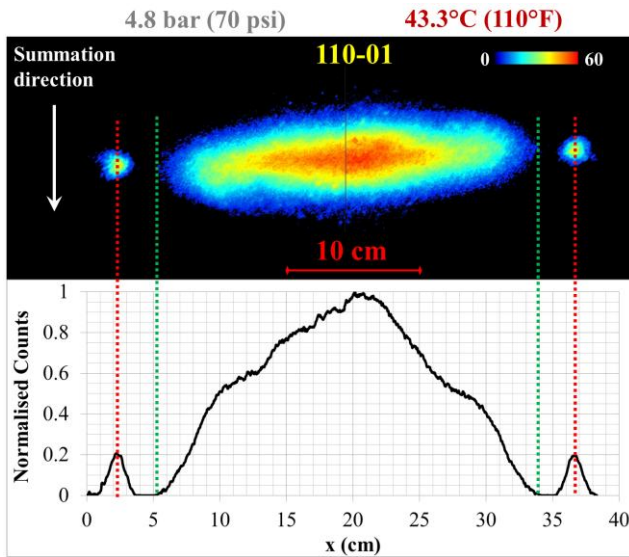


Figure 10. 2-D spray distribution profile and its corresponding summed 1-D profile.

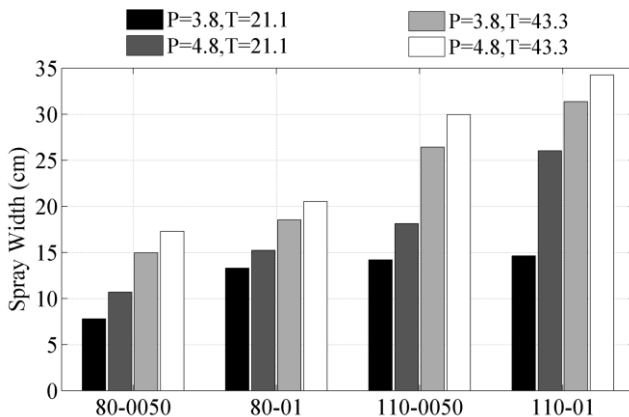


Figure 11. Edge peak to peak distances for all tests.

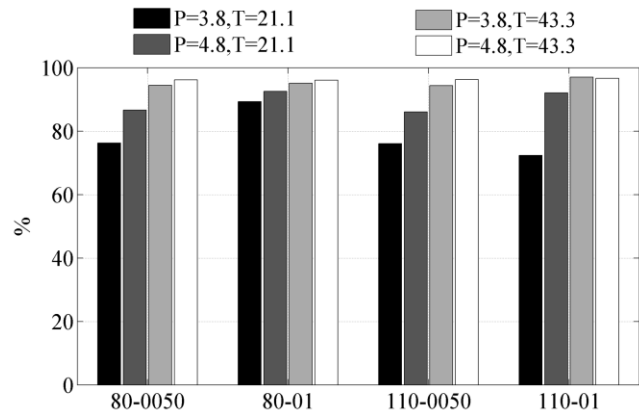


Figure 12. A percentage of spray coverage without heavy edging (EF%).

PIV

Figures 13 and 14 show average velocity vector maps and instantaneous images captured from PIV for 80-0050 and 110-01 nozzle at 21.1°C. In contrast to the point velocity measurements of the PDPA which takes measurements at discrete points; PIV gives velocity measurements across the whole spray plume at once, assigning a vector to the average movement of particles in a specified area. Additionally, PIV allowed for velocity calculations in the heavy edged region of the spray. However, the tradeoff of using PIV is that the vector attributed to the average speed of droplets in the specified matrix is skewed to give a volumetrically disproportionate weighting towards the velocity of the larger droplets. That resulted in giving an inflated velocity measurement when compared to the PDPA velocity values seen in Table 2.

CFD Results

Figures 15-18, show the CFD results with the 110-01 nozzle at 4.8 bar and 43.3°C compared with HSV images. Figure 15 shows relatively good agreement in the spray formation process. One noticeable difference is that the fan angle is underestimated in CFD, as clearly seen in Figures 16-18. The CFD result seen in Figure 16 shows some hints of heavy edging present in the simulation.

Figures 17 and 18 show that CFD velocity profiles are consistent with results from PDPA. Average velocity at $t_{CFD}=0.03$ s, through the midline was 6.3 m/s. The velocity value from PDPA reported in Table 2 was 5.9 m/s.

Further improvement to the CFD model will be performed to get the fan spray angle match to experimental results. In addition, more cases will be modelled focusing on the cases with a surface below the nozzle.

Conclusions

This work investigated effects of heating oil on spray quality. Various flat fan nozzle capacities and spray angles were investigated and in all cases confirmed better transfer quality can be achieved with heated oil. In terms of transfer efficiency, preliminary observations show that increases in pressure and temperature decrease the transfer efficiency. This is due to an increase in material loss to free roaming, small droplets. Further data is required to quantify the total transfer loss.

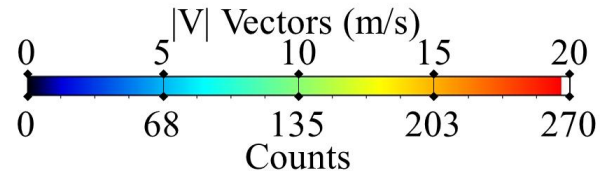
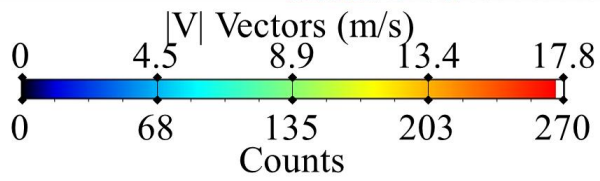
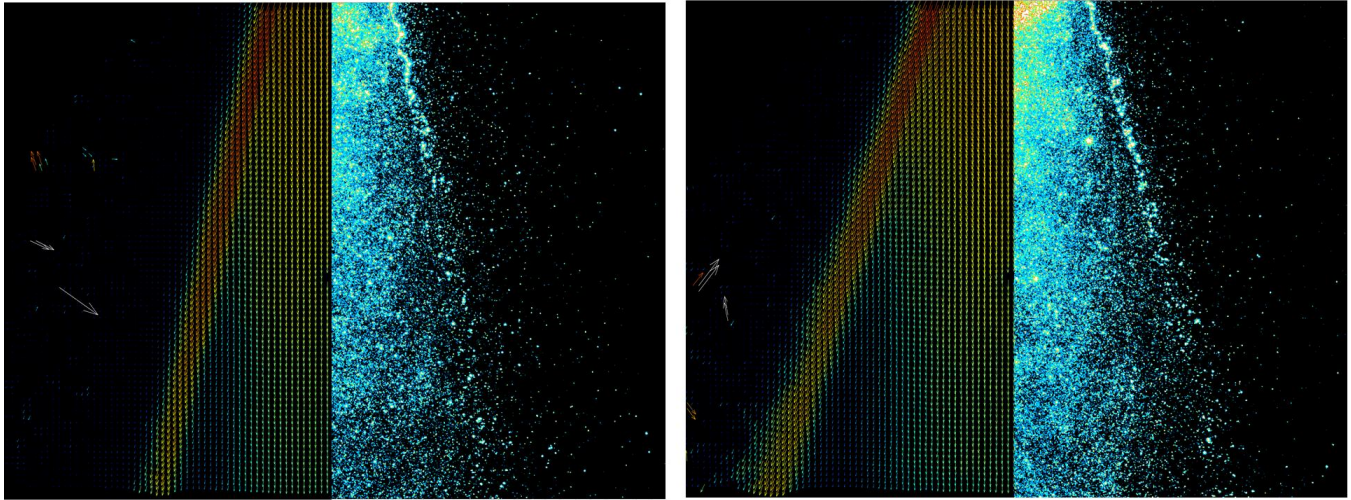
A CFD simulation was conducted to obtain approximate liquid volume fractions and velocities of the flat spray. It was loosely validated with high speed imaging, by comparison of the developing spray.

References

1. South Coast Air Quality Management District, Spray Equipment Transfer Efficiency Test Procedure for Equipment User, May 1989.
2. N. Tamaki et al, Enhancement of Atomization of High Viscous Liquid Jet by Pressure Atomized Nozzle, Proceedings ILASS- Europe Conference, Sept. 2002.
3. Lefebvre, A. H., *Atomization and Sprays*, Hemisphere, New York, 1989.
4. ANSYS FLUENT 15 - Theory Guide, ANSYS, Inc., Canonsburg, PA, 2013.

3.8 bar
(55 psi)

4.8 bar
(70 psi)



Velocity Magnitude (15.24 cm from the nozzle tip)

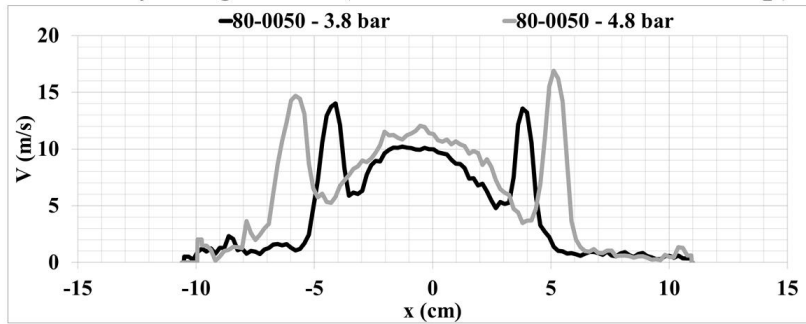
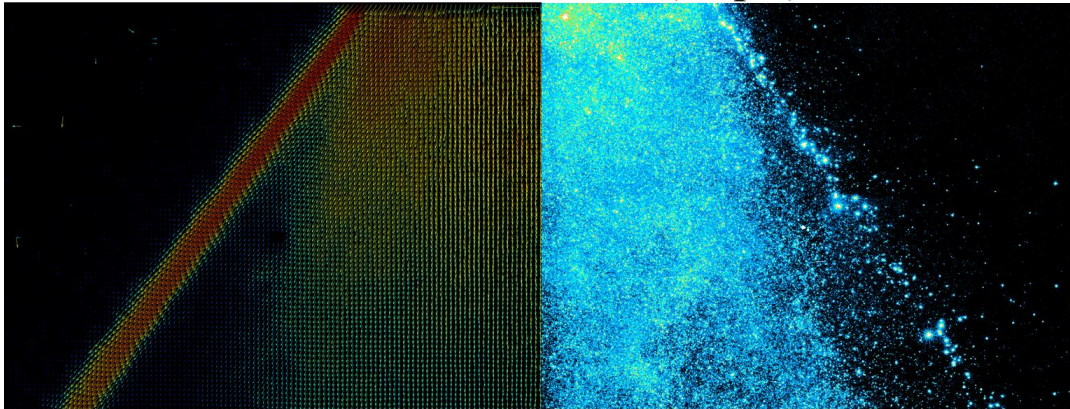
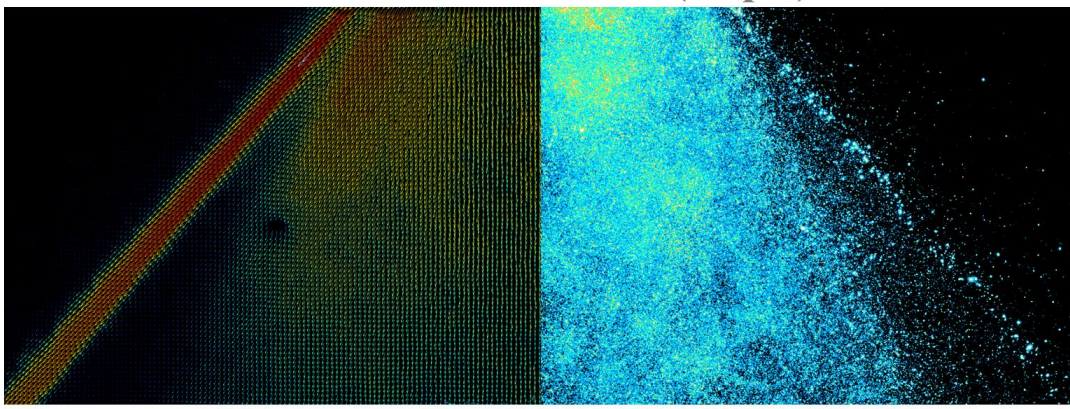


Figure 13. Time averaged velocity and spray distribution for 80-0050 nozzle at 21.1°C obtained via PIV.

3.8 bar (55 psi)



4.8 bar (70 psi)



Velocity Magnitude (15.24 cm from the nozzle tip)

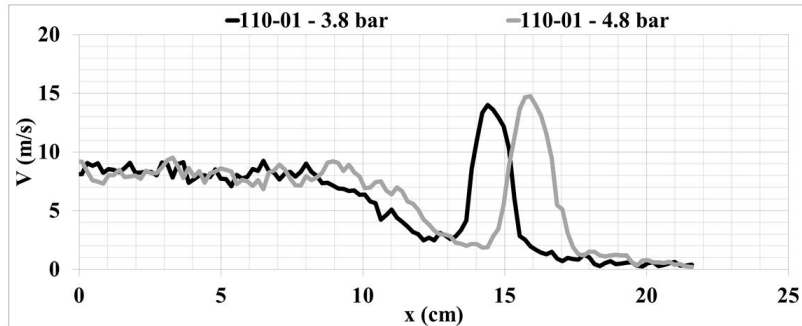


Figure 14. Time averaged velocity and spray distribution for 110-01 nozzle at 21.1°C obtained via PIV. Notice: Half of the spray fan was captured.

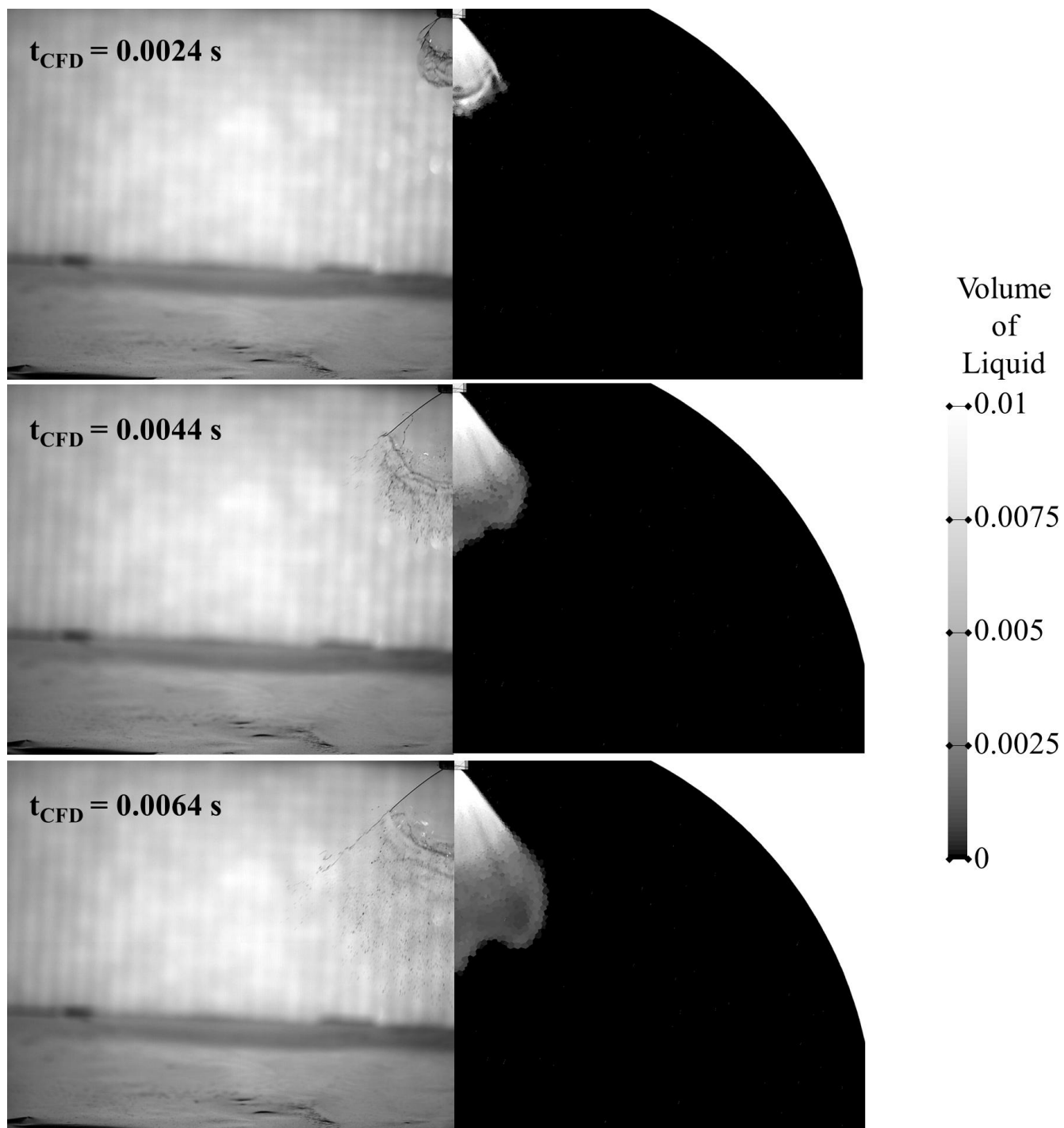


Figure 15. Initial stages of nozzle 110-01 spray at 4.8 bar and 43.3°C.

Left: Frames from high speed imaging
 Right: CFD results, Liquid Volume of Fluid.

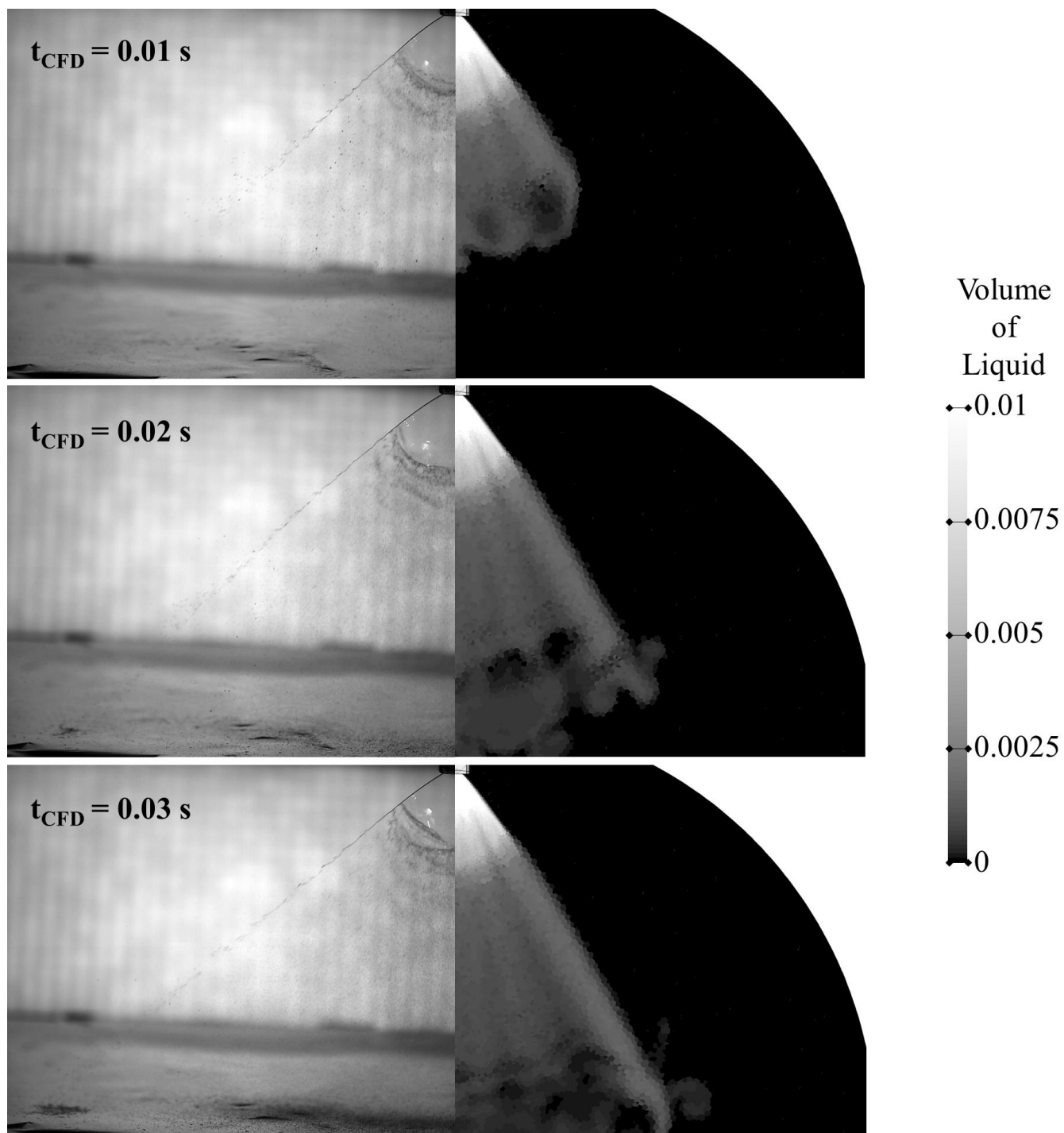


Figure 16. Stages of liquid reaching plane 15.24 cm from 110-01 nozzle at 4.8 bar and 43.3°C.

Left: Frames from high speed imaging
 Right: CFD results, Liquid Volume of Fluid.

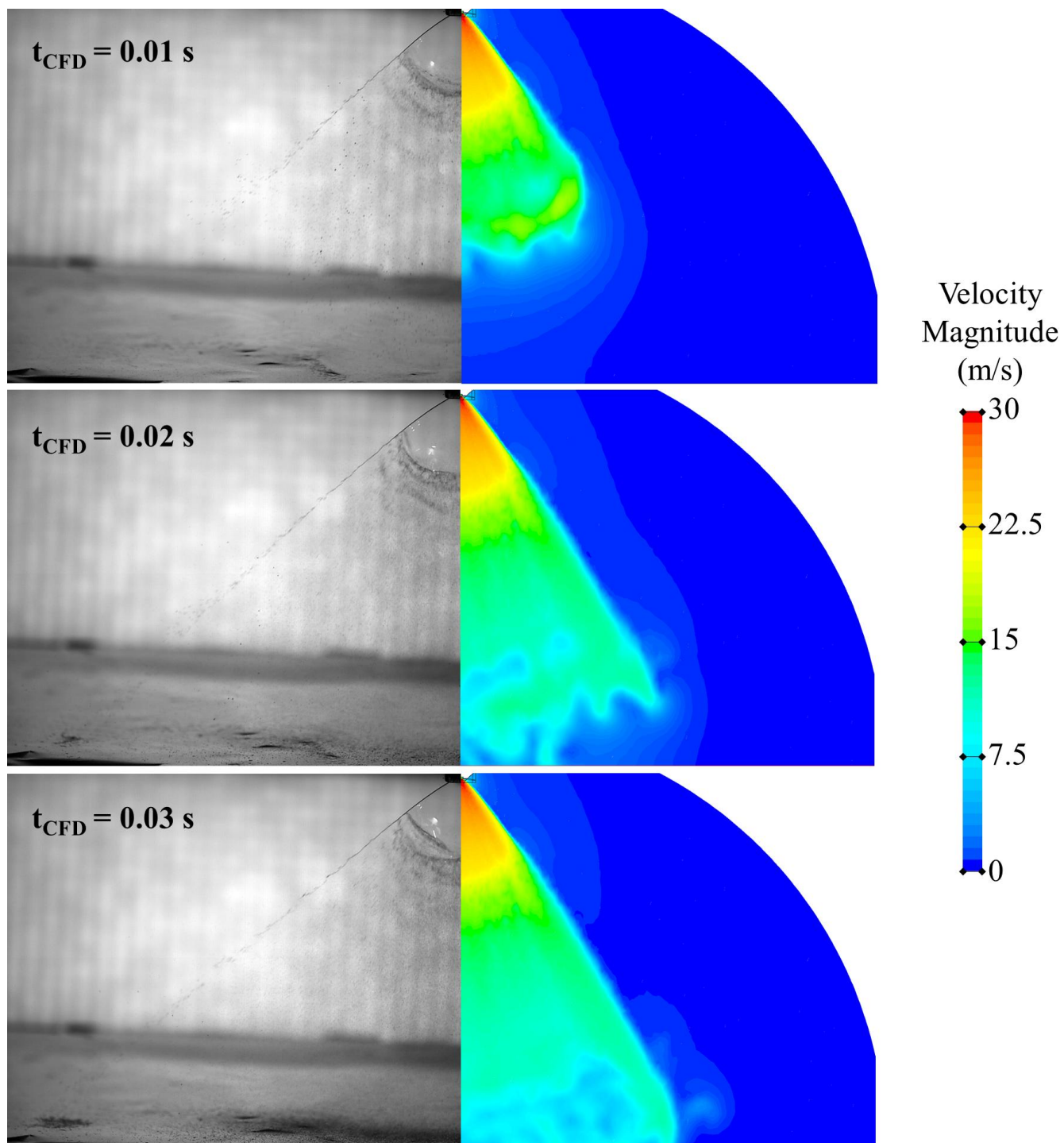


Figure 17. Stages of liquid reaching plane 15.24 cm from 110-01 nozzle at 4.8 bar and 43.3°C.

Left: Frames from high speed imaging
 Right: CFD results, Fluid velocity magnitude.

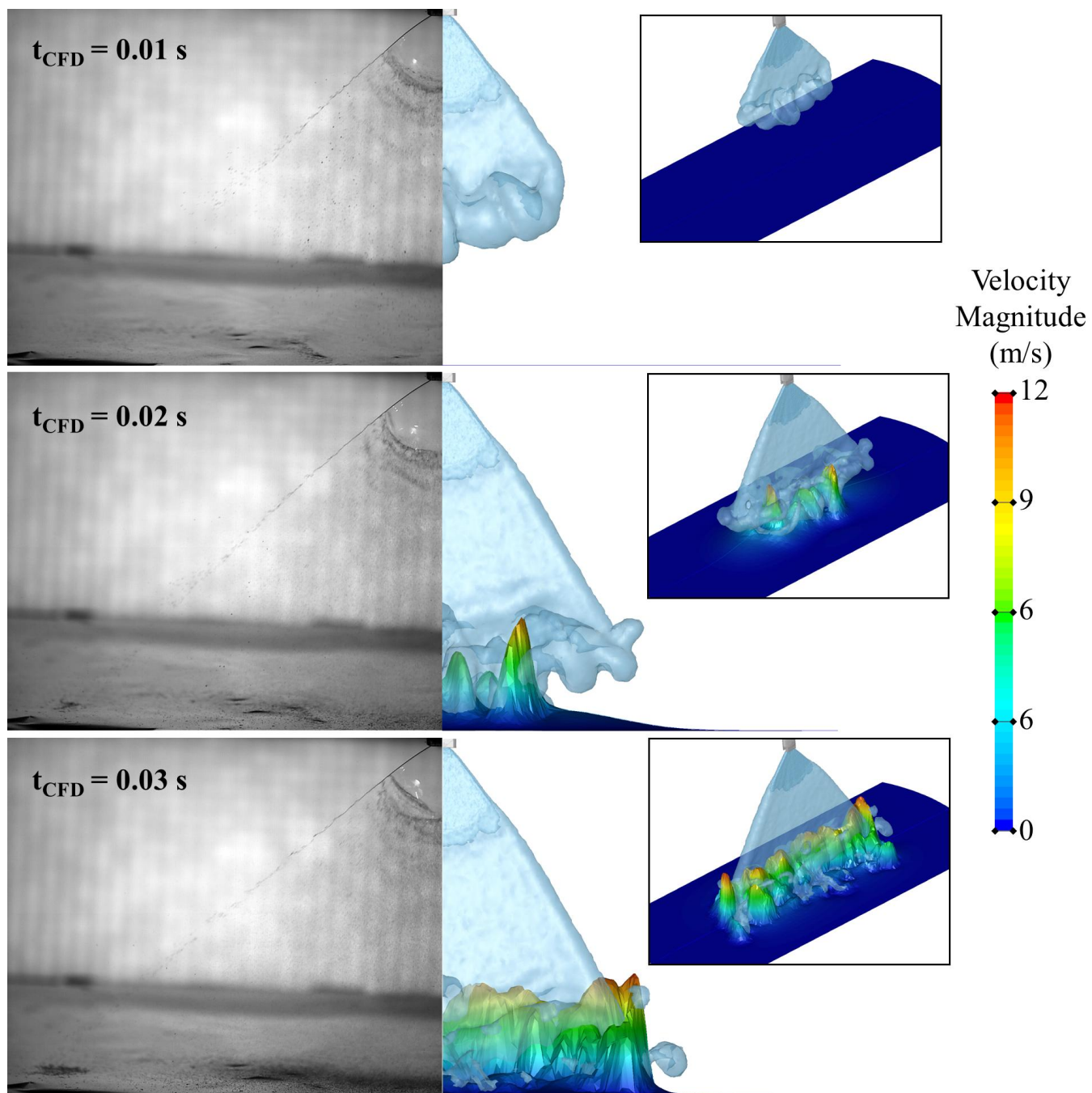


Figure 18. Stages of liquid reaching plane 15.24 cm from 110-01 nozzle at 4.8 bar and 43.3°C.

Left: Frames from high speed imaging

Right: CFD results, Velocity at the plane 15.24 cm away from nozzle.